34rd Symposium on Naval Hydrodynamics
Washington, DC, USA, June 26 - July 1, 2022

DNS Data-Driven Modeling of Turbulent Flows over Rough Walls

G. J. Brereton, J. Yuan (Michigan State University, USA),
M. Aghaei Jouybari (Johns Hopkins University, USA)

ABSTRACT

An extensive direct numerical simulation (DNS) and experimental channel-flow database with 45 different rough surfaces (Aghaei Jouybari et al., *J. Fluid Mech.*, **912**, 2021) are used to distill principal information of the rough-wall flow for modeling the roughness sublayer in a Reynolds-averaged Navier-Stokes (RANS) framework. Three sublayer models are compared, including the roughness-specific wall-function model and the sublayer velocity-profile model, both introduced by Brereton et al., *Phys. Fluids*, **33** (2021), as well as a sublayer body-force model based on a quadratic drag law. All three models were constructed using a zero-plane displacement and an equivalent sand-grain roughness, obtained from the roughness database. Predictions of the friction coefficient are compared with the values deduced from DNS in channel flows at $\mathrm{Re}_\tau = 1000$ on four different rough surfaces. Results from all three sublayer models are in very good agreement with the DNS results. While the wall-function and velocity-profile models are well suited to applications in attached flows at zero or small pressure gradients, the body-force model appears to have significantly more potential for application in complex flows such as those with strong adverse pressure gradients, surface curvature or separation.

INTRODUCTION

The prediction of effects of arbitrarily rough surfaces on the mean velocity field in turbulent flow is a long-standing challenge for turbulence modelers and has many practical applications. When contrasted with modeling of smooth flat-wall boundary layers, in which only the tangential viscous stress $\mu\partial\bar{u}/\partial y$ is exerted by the fluid on the wall, this shear stress is both modified by the flow and supplemented by the roughness-induced form drag force per unit area, caused by the flow-induced pressure distribution around each surface roughness element. The combination of these effects and of any blockage caused by roughness elements must therefore be modeled for rough-wall applications. In most of the modeling approaches developed to date, such as RANS turbulence closures (e.g. Knopp et al. (2009) and Aupoix (2007)) and wall-modeled large-eddy simulations (e.g. Saito et al. (2012)) and Meneveau (2020)) the surface roughness is quantified by a single lengthscale (i.e. the equivalent sandgrain height k_s) within a closure relationship. An empirical calibration is then sought so that predictions made with the roughness model, together with any other required turbulence closures, match approximately selected reference data—usually for sandgrain roughness.

One shortcoming of modeling roughness as a single lengthscale is that, while the model is typically calibrated to predict the wall shear stress correctly, the mean velocity profile within the roughness sublayer is not necessarily correct. This poses challenges, especially for modeling of rough-walled boundary layers with adverse pressure gradients where accurate prediction of the mean separation point is important, or flows with near-surface heat and mass transfer. Inaccuracy in the modeled velocity solution arises in the sublayer—the region extending from the deepest troughs of the roughness at $y = 0$ to just beyond its crest elevation (or peak-to-trough height, denoted as k_c or k_c^+ in viscous units)—where the double-averaged linear momentum equation (Raupach and Shaw, 1982)

$$\begin{aligned}\frac{\partial\langle\bar{u}_i\rangle_s}{\partial t} + \langle\bar{u}_j\rangle\frac{\partial\langle\bar{u}_i\rangle_s}{\partial x_j} \\ = -\frac{1}{\rho}\frac{\partial\langle\bar{p}\rangle_s}{\partial x_i} \underbrace{-\frac{\partial\langle\overline{u_i'u_j'}\rangle_s}{\partial x_j}}_{\text{I}} \underbrace{-\frac{\partial\langle\widetilde{u}_i\,\widetilde{u}_j\rangle_s}{\partial x_j}}_{\text{II}} \\ +\nu\,\nabla^2\langle\bar{u}_i\rangle_s \underbrace{+\langle f_i\rangle_s}_{\text{III}}\end{aligned} \tag{1}$$

contains additional terms II and III compared to its smooth-wall counterpart. Here, $\overline{(\cdot)}$ indicates time averaging, $()'$ indicates turbulent fluctuation from the local time averaged value, $\langle\cdot\rangle_s$ signifies superficial

spatial area averaging, wherein the y-dependent fluid variable is averaged per unit total planar area, rather than per unit fluid planar area (i.e. intrinsic spatial averaging, denoted by $\langle\cdot\rangle$). The intrinsic and superficial spatial averaging operations yield different averages only at y locations below the roughness crest k_c. $\widetilde{(\cdot)} = \overline{(\cdot)} - \langle\overline{(\cdot)}\rangle$ is the spatial heterogeneity of a time-averaged quantity, termed the dispersive or form-induced fluctuations. Specifically, term II is the superficially-averaged dispersive stress and term III is the total forcing of roughness. The streamwise component of the roughness forcing $\langle f_x\rangle_s$ contains the pressure ($-\langle\partial\widetilde{P}/\partial x\rangle_s$) and viscous drag ($\nu\langle\nabla^2\widetilde{u}\rangle_s$) components induced by roughness. No general closures for these additional terms have been proposed. Data from existing DNS of synthetic sandgrain roughness (Yuan & Piomelli, 2014) showed that the y-derivatives of $\langle\overline{u'v'}\rangle_s$ and $\langle\widetilde{u}\,\widetilde{v}\rangle_s$ are of the same order of magnitude within the roughness sublayer and are both much larger than their values in the outer layer. This observation indicates that terms I-III cannot be ignored within the roughness sublayer but must be modeled in a rough-wall closure, either separately or as their combined effect.

The prospect of modeling each of terms I-III in terms of local flow variables and surface topography for arbitrarily rough surfaces seems most unlikely. It is because the infinite variety of different surface roughness topographies are associated with many different effects within the roughness sublayer, such as: recirculating flow patterns isolated from the outer flow, in d-type roughness; recirculation directly behind, and interaction with the outer flow further downstream of roughness elements in k-type roughness; modifications of these flow patterns through the mutual sheltering of roughness elements; enhancement of streamwise vortices near roughness crests; enhanced turbulence production in the wake of certain roughness elements; enhanced redistribution/isotropization of turbulent kinetic energy components in the roughness sublayers; amplification of turbulent motions by interaction between the roughness sublayer and outer eddies; and reduction of turbulence scales by sublayer roughness (Brereton et al., 2021). It follows that, for some arbitrarily rough surface, it is very difficult to anticipate which flow phenomena or combinations thereof might be present in the sublayer, let alone propose how the turbulent and roughness-induced features of such a flow might be modeled accurately in terms I-III. Instead, the most practical technique for modeling flows over surfaces of arbitrary roughness appears to be to develop a database of flowfields computed by DNS, for flows over many different kinds of rough surfaces. The database is then used to infer for different kinds of roughness—often using machine-learning—the roughness-sublayer velocity profile $\langle\bar{u}_i\rangle_s$ found from the DNS solutions to rough-wall flow. RANS Eq. (1) is then integrated from the edge of the roughness sublayer outwards, where terms I-III are almost zero, to determine the rest of the velocity profile $\langle\bar{u}_i\rangle_s$. This approach seems preferable to trying to infer the forms of models for terms I-III for a given rough-wall flow and integrating Eq. (1) over the entire domain to determine $\langle\bar{u}_i\rangle_s$.

In this paper, we discuss the construction of a 45-surface database and the representation of different rough-wall flows through zero-plane displacement heights and equivalent sand-grain roughnesses, which are useful for mapping information on roughness flow resistance into rough-wall flow closure models. We also present RANS modeling approaches in which we model rough-wall flow using: *i*) roughness-specific wall functions; *ii*) velocity profile models which extend through the roughness sublayer; and *iii*) a roughness-specific surface-layer body-force model based on a quadratic drag law; while modeling the turbulent stresses beyond the roughness sublayer as their smooth-wall counterparts. We conclude by considering the suitability of such wall functions and drag laws for application in more complex flows.

DNS DATABASE OF ROUGH-WALL TURBULENT CHANNEL FLOW

The database was constructed by solving the incompressible Navier-Stokes equations by direct numerical simulation in turbulent half-channel flow at $\mathrm{Re}_\tau = u_\tau h/\nu = 1000$, where $u_\tau = \sqrt{\tau_w/\rho}$ is the friction velocity and h is the channel half-height. An immersed boundary method was applied at the rough wall to enforce fine-grained boundary conditions of no slip/no penetration for the particular rough-surface geometry chosen, on a non-conformal Cartesian grid. The concept of minimal-span channel was used to limit computational cost (Jimenez and Moin, 1991; Chung et al., 2015). Forty five different rough surfaces, the surface coordinates of which could be readily generated computationally, were chosen to represent sandgrain roughness, sinusoidal roughness, arrays of hemispheres on otherwise smooth surfaces, surface elevations described by random (white noise) Fourier modes, *etc*. Only the DNS cases (30 out of 45) that were considered fully rough were kept for k_s modeling. The fully rough regime was considered to have been reached

if the value of k_s obtained from the roughness function was such that $k^+ \geq 50$. Data from 15 other fully rough flows with different roughnesses, obtained from previous experiments, were added to the collection. A detailed description of the surfaces and the way in which they were generated is given by **?**.

The number of grid points (n_x, n_y, n_z) used was 400, 300 and 160 in the respective directions, with a uniform mesh of sizes $\Delta x^+ = 7.5$ and $\Delta z^+ = 6.3$ in the x- and z-directions. A stretched mesh was employed in the wall-normal y-direction so that the third grid point from the lowest point (deepest roughness trough) was at $y^+ < 1$ and the y grid size at the channel center was $\Delta y^+ = 9.5$. In order to carry out DNS simulations of flow over many different rough surfaces at the lowest reasonable computational cost, the minimal-span channel approach (Jimenez and Moin, 1991; Chung et al., 2015; MacDonald et al., 2017) was adopted. In this approach, the reduced domain size in the spanwise direction compromises the accuracy of some outer-flow statistical measures, but resolves the essential near-wall turbulence dynamics, mean velocities, friction velocity and stresses accurately as far from the wall as $y/h \simeq 0.3$.

For each kind of roughness considered, the very different mean velocity profiles were all found to exhibit log-linearity when shifted by the zero-plane displacement height d, and so could be matched to $u^+ = (1/\kappa)\ln(y^+ - d^+) + B$, where B is a roughness-specific velocity offset. The equivalent sandgrain roughness k_s—a rough-wall flow-dependent lengthscale—was also deduced for each roughness, using the experimental correlation: $u^+ = (1/\kappa)\ln(y/k_s) + 8.5$ (Nikuradse, 1933). Thus, for each kind of roughness, the flow lengthscale k_s, displacement d, velocity offset B, and the multiple roughness topography lengthscales (mean height, rms height, mean absolute height variance, mean effective slopes), the surface porosity and the roughness skewness and kurtosis were determined. **?** have shown how deep neural network and Gaussian process regression machine-learning methods can be used to train models to predict k_s from the roughness parameters of a surface, with discrepancies between the machine-learning model estimates and the original DNS data values of k_s of less than about 10%, for any roughness with topographical parameters within the ranges of the data set. The data and models are archived at https://github.com/MostafaAghaei, where interested researchers can evaluate machine-learning-estimated values of k_s in fully-rough flow from the roughness parameters of their own particular surfaces.

ROUGHNESS SUBLAYER MODELS

For steady, attached, fully-rough wall-bounded flows at or close to equilibrium, the DNS database can be used in several ways to model rough-wall flow. When the mesh is sufficiently coarse that the wall-adjacent cell's center is within the log-linear region, a conventional wall function can be deduced from the database for any specific roughness. For finer grids with multiple cells within the roughness sublayer, an algebraic sublayer velocity profile can be inferred from the database for any particular roughness. It is also possible to model the drag force exerted by the surface roughness through a quadratic velocity-dependent body force opposing motion in the wall-adjacent layer of cells, as $f_x = -\alpha_t|u|u$, where the turbulent roughness reciprocal lengthscale α_t is calibrated using the equivalent sandgrain height k_s of the rough surface, as provided by the database. We present results for each of these models below, when they are combined with an outer-flow k-ϵ closure with finite-volume discretization and a standard elliptic Navier-Stokes equation solver, typically with 50 to 100 points in the wall-normal direction, for surface roughnesses of the sandgrain type and of very different types.

Test surfaces

The test surfaces considered to evaluate roughness sublayer models were: *i*) sandgrain roughness with peak-to-trough height in wall units $k_c^+ = 90$; *ii*) a uniformly-spaced array of half-ellipsoids of height $k_c^+ = 90$ on a smooth surface; *iii*) a two-dimensional sinusoidally wavy surface of height $k_c^+ = 60$; and *iv*) random (white noise) low-order spatial Fourier modes of height $k_c^+ = 120$. These surfaces corresponded to cases C37, C17, C30, and C40 respectively in the DNS database. They were chosen because they were considered to be in the fully-rough regime at $\mathrm{Re}_\tau = 1000$ and their different topographies yielded quite different sublayer velocity profiles. The prospect of predicting them by other modeling approaches appears to be remote. The surfaces are shown in Figs. 1(a) to (d) together with their DNS-resolved near-surface velocity profiles. In the present immersed boundary method, the immersed fluid-solid interface is contained by a marker function $\phi(x, y, z)$ defined as the fraction of fluid volume in each computational cell. The rough surfaces were visualized as iso-surfaces corresponding to a cell fluid fraction of 0.5, which is expected to show cell-wise steps if the immersed interface is not aligned with cell borders (e.g. in Figs. 1(d)). A more

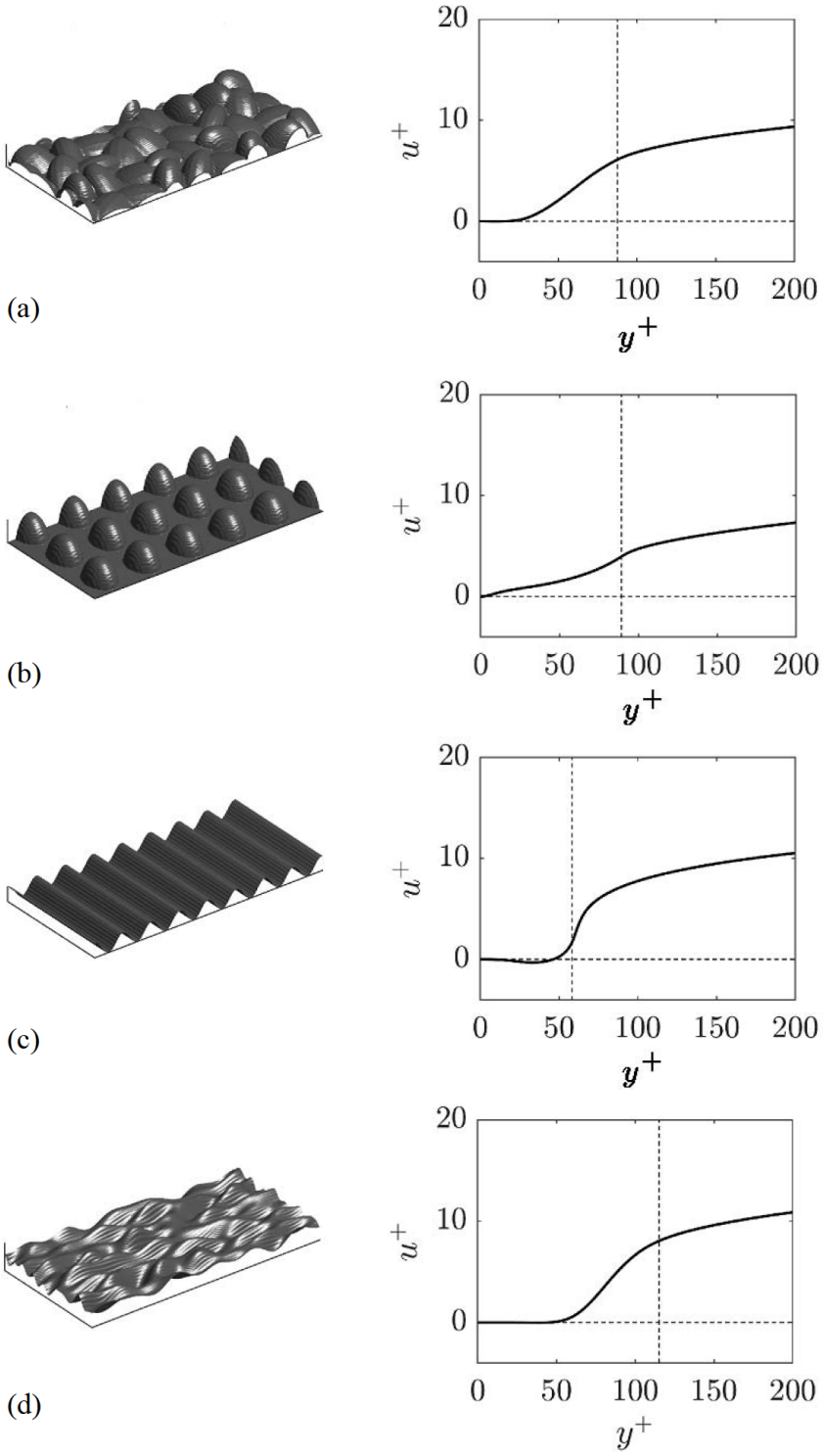

Figure 1: Inner profile of $\langle \bar{u} \rangle_s^+$ for flow over four rough surfaces: (a) a simulated sandgrain roughness of height $k_c^+ = 90$, (b) a uniformly-spaced array of semi-ellipsoids of height $k_c^+ = 90$, (c) a two-dimensional sinusoidally wavy wall of height $k_c^+ = 60$, and (d) composite of random (white noise) Fourier modes of height $k_c^+ = 120$. All cases were at $\mathrm{Re}_\tau = 1000$, computed by half-channel DNS; ------ (vertical) roughness crest height k_c^+.

Table 1: Channel-flow computations of C_f at $\mathrm{Re}_\tau = 1000$ with roughness-specific wall functions. C_f obtained by DNS is compared with C_f predicted with the wall-function (WF) model and with the wall-function model when B was found with a machine-learning (ML) procedure. d is defined as the centroid location of the y profile of roughness forcing $\langle f_1 \rangle_s$.

Surface	k_c^+	B	d^+	k_s^+	C_f DNS	C_f WF	C_f ML
Sandgrain	90	-3.40	46	109	0.0156	0.0147	0.0145
Semi-ellipsoids	90	-5.40	44	260	0.0216	0.0209	0.0209
Two-dimensional sine wave	60	-2.20	54	64	0.0128	0.0119	0.0118
White-noise Fourier modes	120	-1.50	70	50	0.0116	0.0109	0.0107

sophisticated surface reconstruction from ϕ than using the isosurfaces of $\phi = 0.5$ may yield smoother visualizations but was not attempted.

Roughness-specific wall function

In a velocity wall-function approach, the velocity at the center of the wall adjacent cell is denoted as $u_c(y_c)$ and the grid is chosen to be sufficiently coarse that y_c can be assumed to be within the log-linear region of a steady, attached flow. The effective viscosity ν_w to be applied in the cell adjacent to the wall is set to equate the wall shear stress there, where the velocity is modeled as locally linear, to that at y_c in the log-linear region, *i.e.*

$$\frac{\tau_0}{\rho} = \nu_w \frac{\bar{u}_c}{y_c} = u_\tau^2 \tag{2}$$

and

$$\frac{\bar{u}_c}{u_\tau} = \frac{1}{\kappa} \ln(y_c^+ - d^+) + B, \tag{3}$$

so that

$$\nu_w = \frac{y_c u_\tau}{(1/\kappa)\ln(y_c^+ - d^+) + B}\,. \tag{4}$$

The solver uses the returned value of $\bar{u}_c/u_\tau$ at y_c^+ to refine its estimate of u_τ through iteration, or combines Eq. 3 with a model relation between u_τ and $\sqrt{k}$ to determine an approximation to $\bar{u}_c/u_\tau$ directly. In this way, the wall shear stress is made to take the value required by the assumed form of the log-linear velocity at y_c. Consequently the requirement that y_c is no closer to the wall than the inner extent of the log-linear region places a *lower* limit on the mesh size.

Using the DNS-determined values of d^+ and B in the wall function for each kind of roughness, coupled with a standard k-ϵ outer-flow closure, in a channel-flow computation at $\mathrm{Re}_\tau = 1000$, agreement to within 7% was found between the DNS-determined and wall-function (WF) modeled values of the friction coefficient C_f, shown in Table 1. Since $C_f = \tau_0/(\frac{1}{2}\rho\bar{U}^2)$ (where $\bar{U}$ is an outer velocity scale) and the wall-function coefficients were determined from DNS—to ensure the correct wall shear—this agreement effectively confirms that, with the correct rough-wall model, the k-ϵ closure predicts the *rest* of the velocity field, and so $\bar{U}$, accurately to achieve this agreement. When the values of B and d^+ were determined by providing the rough-surface values of mean and rms roughness height, absolute height variance, effective slope, etc. as inputs to a machine-learning (ML) model trained against DNS results for all 45 different rough-surface flows, according to the particular values of those roughness parameters, the prediction of C_f was typically 1% or 2% worse than that when B and d^+ were found from DNS data for each particular rough-surface flow.

The shortcoming of wall-function models is that they rely on a relation between the wall friction and flow in a log-linear overlap region which is found in steady, attached, flat-wall boundary layers; it may have little relevance to other flows (Wilcox, 1993). It is therefore attractive to explore modeling approaches which do not rely on properties of an overlap layer, but exploit the influence of the roughness sublayer more directly on the outer flow. Two such approaches are described below.

Roughness-specific sublayer velocity profile

The sublayer velocity profile approach requires an algebraic model of the roughness-specific sublayer velocity profile, in wall units. This algebraic model

Table 2: Channel-flow computations of C_f at $\mathrm{Re}_\tau = 1000$ with sublayer velocity-profile models. C_f obtained by DNS is compared with the C_f model prediction when the parameters of the roughness sublayer velocity profile are prescribed from DNS data.

Surface	k_c^+	B	d^+	y_0^+	y_l^+	$C_{f_{\mathrm{DNS}}}$	$C_{f_{\mathrm{Model}}}$
Sandgrain	90	-3.40	46	25	86	0.0156	0.0160
Semi-ellipsoids	90	-5.40	44	0	105	0.0216	0.0228
Two-dimensional sine wave	60	-2.20	54	43	84	0.0128	0.0129
White-noise Fourier modes	120	-1.50	70	50	110	0.0116	0.0121

reflects the effect of a particular roughness on the roughness-sublayer double-averaged mean velocity profile. The velocity profile can be determined directly from a roughness-resolved DNS or obtained through some correlation based on characteristics (e.g. lengthscales) of the roughness geometry; the former approach was employed here. When rescaled by the inferred friction velocity during a computation, this partial velocity profile, which typically extends from $y = 0$ to the edge of the roughness sublayer, yields the sublayer profile of $\langle\overline{u}\rangle(y)$. Its gradient is imposed on the relevant terms in the otherwise unmodified k and ϵ equations so they will, when solved, yield reasonable estimates of k and ϵ at the edge of the roughness sublayer. The outer flow is then solved with these values of $\langle\overline{u}\rangle$, k and ϵ as boundary conditions at the edge of the roughness sublayer. The algebraic profile model is determined from the DNS mean velocity field, shown for four different roughnesses in Figs. 1(a) to (d). Each sublayer profile is modeled as a zone of zero/negligible velocity, extending from $y = 0$ to y_0^+, blended to the inner limit of the log-linear region at y_l^+. The values of y_0^+ and y_l^+ are given in Table 2 for each specific roughness. The blending function was a cubic polynomial, the coefficients of which were chosen as the required conditions on $\langle\overline{u}\rangle^+$ and $d\langle\overline{u}\rangle^+/dy^+$ at $y^+ = y_0^+$ and $y^+ = y_l^+$. Additional details of this modeling approach are provided by Brereton et al. (2021).

It can be seen from Table 2 that the values of C_f predicted by the sublayer velocity profile model (given the correct values of y_0^+ and y_l^+) agree with the DNS-determined values to within about 5%. In companion predictions of synthetic sandgrain roughnesses of heights $k_c^+ = 28$ and 86, shown in Fig. 2, it can be seen how the zero-velocity and cubic parts of the prescribed sublayer profile match the DNS data, blend smoothly with the outer computed log-layer, and that the outer-flow k-ϵ predictions of $\bar{u}$ are in good agreement with the DNS velocity profile data. Thus the specification of the velocity profile across the roughness sublayer from DNS data for a particular kind of roughness appears to provide sufficient information to predict the entire boundary layer with a standard RANS closure. In these test cases, the values of y_0^+ and y_l^+ were determined by inspection. However, they could also be correlated to lengthscales of the particular roughness geometry in a machine-learning model, as was done with the values of k_s^+ (or equivalently B).

Surface-layer body force drag model

The roughness body force $\langle f_i\rangle_s$ in Eq. (1) is a pseudo body force per unit mass which describes the effects of viscous and form drag within the roughness sublayer. In fully-developed channel flow, it can be shown that

$$\tau_0 = \rho \int_0^{k_c} \langle -f_x\rangle_s \, dy + \mu \frac{\partial\langle\bar{u}\rangle_s}{\partial y}\bigg|_0 . \qquad (5)$$

At sufficiently large Reynolds numbers, the contributions of both the explicit viscous term and the viscous part of $\langle f_x\rangle_s$ become negligible and the flow is termed 'fully rough.' The simulations of Yuan and Piomelli (2014), for flow over surfaces made up of densely distributed ellipsoidal grains, indicate that the shear of double-averaged velocity $\partial\langle\bar{u}\rangle_s/\partial y \simeq 0$ at $y = 0$, as the mean velocity in the lower portion of the roughness sublayer was almost zero. It follows that τ_0 can then be modeled as the integral of $\langle -f_x\rangle_s$. Although the $\langle -f_x\rangle_s$ profile can be determined from DNS data and readily modeled for sandgrain roughness, as shown in Fig. 3, its shape is quite irregular for other kinds of roughness and ill-suited for general modeling of rough-wall flow (Brereton et al., 2021).

An alternative approach is to model the volume-averaged effect of the local y-profile of

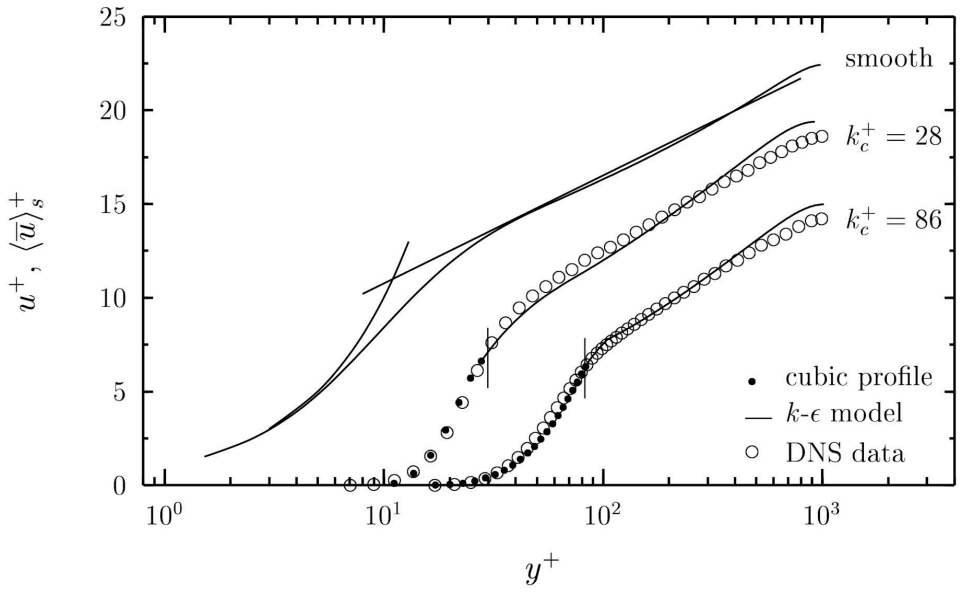

Figure 2: Profiles of mean velocities on smooth (u^+) and sandgrain rough walls ($\langle\overline{u}\rangle_s^+$) at $Re_\tau = 1000$ (Brereton et al., 2021). The profiles modeled from the sublayer velocity profile approach are compared with DNS data from rough-wall flows and with the law of the wall for smooth-wall flow. Short vertical lines indicate the edge of the roughness sublayer.

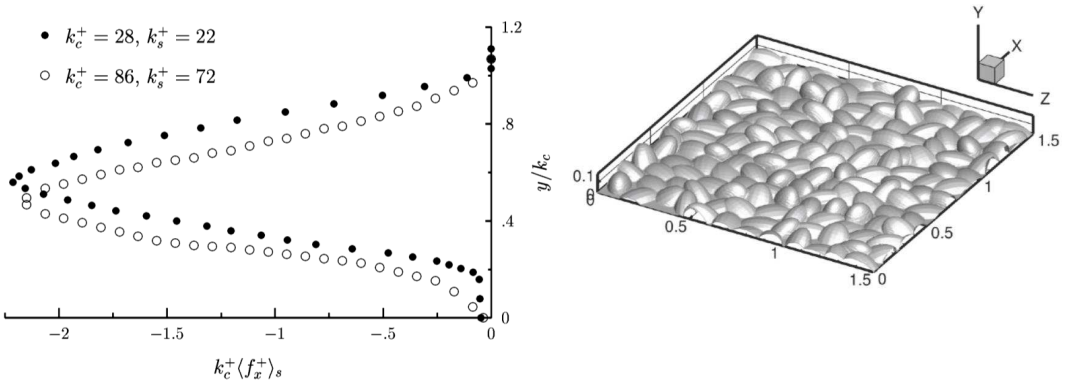

Figure 3: Distributions of the roughness body force $\langle f_x\rangle_s$ across roughness sublayers of a sandgrain roughness with two different crest heights k_c.

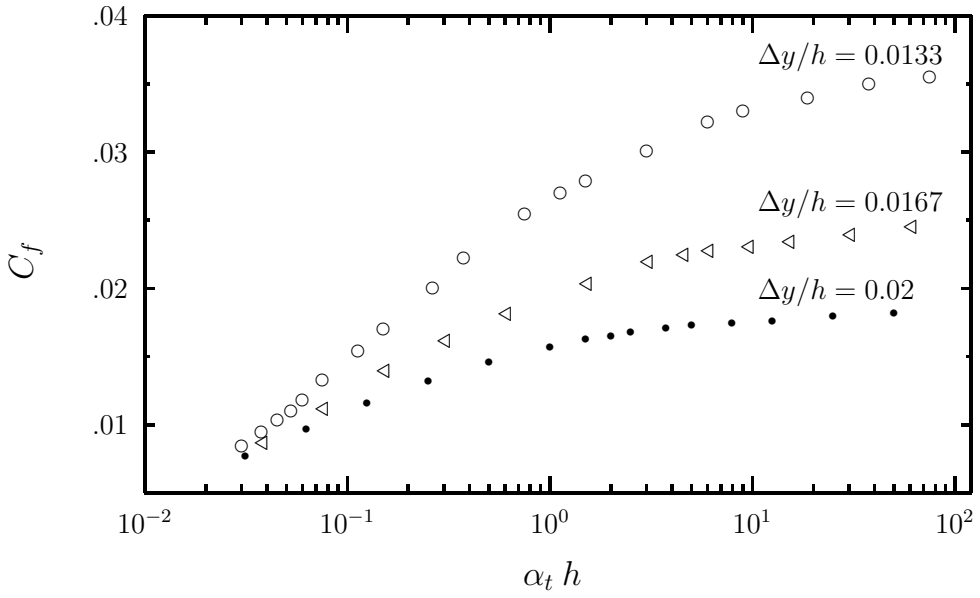

Figure 4: Mapping of C_f against $\alpha_t h$ in turbulent pipe flow at $\mathrm{Re}_\tau = 1000$ for a quadratic drag body-force model of roughness, at different values of the wall grid height $\Delta y/h$, where h is the pipe radius.

Table 3: Channel-flow computations of C_f at $\mathrm{Re}_\tau = 1000$ with a roughness body-force model. C_f obtained by DNS is compared with the C_f model prediction when the DNS-determined value of k_s is mapped to $\alpha_t \Delta y$ when $\Delta y/h = 0.0133$.

Surface	k_s^+	$\alpha_t\, \Delta y$	$C_{f_{\mathrm{DNS}}}$	$C_{f_{\mathrm{Model}}}$
Sandgrain	109	0.0150	0.0156	0.0168
Semi-ellipsoids	260	0.0980	0.0216	0.0206
Two-dimensional sine wave	64	0.0040	0.0128	0.0131
White-noise Fourier modes	50	0.0027	0.0116	0.0118

$\langle f_x \rangle_s$, or more precisely $\langle f_x \rangle_s - \partial \langle \widetilde{u}\,\widetilde{v} \rangle_s / \partial y$ in Eq. (1), over each wall-adjacent cell in a finite-volume computation. Vargese & Durbin (2020) have shown that the quadratic drag model $f_x = -\alpha_t |u| u$ can capture this effect, with α_t calibrated to produce the desired wall friction for each kind of roughness—an approach related to the 'discrete element' model of Taylor et al. (1985).

In the context of a conventional RANS code, we implement this model by specifying an x-momentum source term: $-\alpha_t |u| u$, as the average value of $\langle f_x \rangle_s$ across the wall-adjacent cell of height Δy. In order to estimate the wall shear stress correctly, a new wall function is applied at the center of the wall-adjacent cell, at y_c where the x-velocity is u_c. Thus, for the 'wall function,' $u^+ = (1/\kappa) \ln y^+ + B$ is replaced by

$$u^+ = 1/\sqrt{\alpha_t \Delta y}, \tag{6}$$

so that

$$u_\tau = u_c \sqrt{\alpha_t \Delta y}, \tag{7}$$

$$\tau_0 = \rho u_\tau^2 = \rho \alpha_t u_c^2 \Delta y, \quad \text{and} \tag{8}$$

$$\nu_w = \alpha_t y_c u_c \Delta y. \tag{9}$$

In this wall-layer model, the new wall function effectively sets the velocity at the center of the first cell to $u_c^+ = 1/\sqrt{\alpha_t \Delta y}$ regardless of the value of y_c^+, to achieve the desired wall friction, and the mesh node at $y = 0$ is set to $y = d$. The location of y_c is not constrained by any consideration of log-linearity in an assumed velocity profile. The value of α_t is then calibrated against a roughness measure such as the equivalent sandgrain scale k_s, for a given wall-adjacent cell height Δy, as proposed by Varghese and Durbin (2020). In a more rigorous treatment of such a body-force drag model, one could include the effect of the fluctuating velocity on the role of this body force as an extra production term in the turbulent kinetic energy and dissipation rate equations, as is done in modeling effects of buoyancy (Durbin and Pettersson Reif, 2001). It has not been attempted in this preliminary study.

To calibrate α_t for a particular roughness, the value of k_s was first determined from the DNS rough-wall database or its associated machine-learning model. The Colebrook equation was then used to express k_s as the friction coefficient C_f in pipe flow. The corresponding value of α_t (or $\alpha_t \Delta y$) was then found from a mapping of C_f against $\alpha_t \Delta y$ in pipe flow, computed using the body-force model described above. The resulting value of $\alpha_t \Delta y$, at the chosen grid size Δy, could then, in theory, be applied to the body-force model for prediction of any other near-wall flow. In this calibration, the C_f mapping against α_t was carried out with a standard k-ϵ model in turbulent pipe flow at $\mathrm{Re}_\tau = 1000$, with the x-momentum source term and the wall function as specified above, and is plotted in Fig. 4. It can be seen that the value of $\alpha_t h$ (where h is the constant pipe radius) required to achieve a given C_f depends strongly on the wall grid spacing Δy except in the limit of very small roughness. Moreover, the asymptotic behavior of these curves at large $\alpha_t h$ implies that coarse grids can only be used to model small roughness effects, and smaller values of Δy are required for flow over surfaces of larger roughness.

To test the efficacy of this modeling approach, the values of k_s for each of the four test roughnesses were substituted into the Colebrook (1939) equation:

$$C_f = \left[4 \log \left\{ \frac{k_s/D}{3.7} + \frac{1.255}{\mathrm{Re}_d \sqrt{C_f}} \right\} \right]^{-2}, \tag{10}$$

and used to determine the corresponding C_f in pipe flow. From this value, $\alpha_t \Delta y$ was determined from Fig. 4 at $\Delta y/h = 0.0133$ and used to scale the drag force model in a channel-flow calculation at $\mathrm{Re}_\tau = 1000$ with this grid size. The value of C_f obtained from this calculation is compared with the original DNS determination of C_f in channel flow in Table 3. The agreement is very good—within 7%—even for the high value of α_t required to describe the semi-ellipsoid roughness. While this technique can certainly be calibrated to yield accurate predictions of the DNS-determined values of C_f in a roughness body force model, further explorations are needed to determine how accurately mean velocity profiles can be predicted and whether it is beneficial to distribute the body force over multiple cells.

For general modeling purposes, an algebraic representation of the mapping of Fig. 4 in near-wall variables, as $\alpha_t \Delta y = f(\Delta y^+, k_s^+, \dots)$ is much more desirable. To this end, a series of RANS calculations were carried out in channel flow, with a k-ϵ model with f_x as a source term in the x-momentum equation and the wall function specified as the wall-layer model of this section. From calculations at Re_τ of up to 2000 and $k_s/\Delta y$ from 0 to 3 on meshes with different sizes of Δy, it was found that the value of $\alpha_t \Delta y$ required to produce the body force $f_x = -\alpha_t |u_c| u_c$ that gave the value of C_f corresponding to k_s could be approximated as:

$$\alpha_t \Delta y \simeq \alpha_0 \Delta y + 8\, k_s^+ \Delta y^+ (\alpha_0 \Delta y)^2, \tag{11}$$

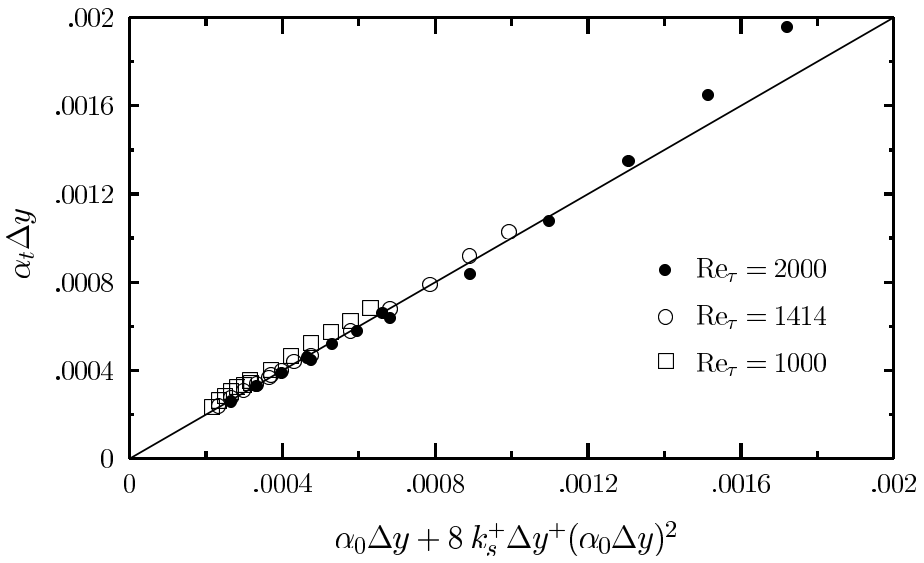

Figure 5: Comparison between RANS-determined values of $\alpha_t \Delta y$ and the linear k_s fit of Eq. 11 in turbulent channel flow for a quadratic drag body-force model of roughness, at different values of Re_τ, k_s and wall grid height Δy. The solid line represents equality between the model and data.

where $\alpha_0 = 0.04$. A comparison between the α_t model of Eq. 11 and the RANS calculated values of α_t that matched C_f at a given value of k_s is shown in Fig. 5.

It can be seen from Fig. 5 that the values of $\alpha_t \Delta y$ are in very good agreement with the algebraic model of Eq. 11. It is interesting to note that the effect of the body force is not evident until α_t exceeds α_0, and that the dependence of α_t on roughness scale k_s^+ appears to be linear over this range of small roughnesses. The former observation may be analogous to the observation of hydraulic smoothness at small roughnesses while the latter is consistent with the asymptotic forms of the curves in Fig. 4 at low values of α_t. This expression for $\alpha_t \Delta y$ is presented tentatively for $\Delta y^+ < 15$ and $k_s^+ < 45$. It is intended to serve as an example of the kind of model calibration that might be established for α_t with considerably more testing. An additive quadratic dependence on k_s^+ appears to be necessary to describe accurately the two largest values of $\alpha_t \Delta y$ in Fig. 5. The much larger roughnesses depicted in Fig. 1 and characterized in Table 3 are beyond the limits of applicability of this linear small-roughness model.

While this surface body force roughness model has been calibrated and tested in fully developed duct flows, the exclusively near-surface nature of the model implies that it may also be equally applicable to developing flows such as boundary layers under various pressure gradients. This hypothesis is currently being tested.

CONCLUDING REMARKS

In this paper, we discuss one use of a database of the results of DNS of turbulent channel flow for 45 different kinds of surface roughness, for fully rough flow at $\mathrm{Re}_\tau = 1000$. These results provide essentially complete details of all aspects of these flows, which could not be deduced with the same accuracy or consistency by other methods. For the purposes of this paper, the information is distilled into a zero-plane displacement and an equivalent sand-grain roughness size for each rough surface, as a preliminary step in developing RANS modeling approaches for flow over surfaces of arbitrary roughness. Machine-learning techniques have also been applied to the database to allow for interpolation of the likely effects of flow over other surfaces with roughness topography parameters similar to those of the 45 constituent flows. By developing this database for so many flows using the same numerical method, convergence criteria, grid size, etc., much of the uncertainty that would otherwise arise when calibrating models against data from multiple sources is eliminated. Similar approaches could be used to develop much-needed databases for smaller roughnesses, flow in the transitionally rough region, and flow in adverse pressure gradients.

The capabilities of three different RANS models for flow over rough walls were explored by comparing their predictions of the friction coefficient C_f with the DNS-deduced values, for four

very different large-roughness surfaces, using only the distilled database information. It was shown that roughness-specific wall-function and sublayer velocity-profile models were in very good agreement (within about 7%) with DNS results. Such models would be well suited to application in flows over macroscopically flat surfaces for which it was known *a priori* that they remain attached, at zero or small pressure gradients.

A roughness body-force model, applied only in the wall-adjacent cell of the mesh, was shown to be equally accurate in determining the friction coefficients of the four test rough surfaces from the distilled database information. Its dependence on exclusively near-surface quantities implies that it may be far more general than other models which rely on an assumption of log-linearity in the mean velocity profile, and for this reason it appears to have significantly more potential for application in complex flows, such as those with strong adverse pressure gradients, surface curvature, or separation. A plausible strategy for modeling roughness in this way would be to: *i*) determine k_s for the surface of interest, as a function of its roughness dimensions, with the machine-learning model provided at https://github.com/MostafaAghaei; *ii*) generate a mesh in which the height of surface-adjacent cells was of the same order as k_s; *iii*) select a suitable α_t model (e.g. Eq. 11); and *iv*) solve the appropriate RANS equations with standard boundary conditions, the surface-cell body force $f_x = -\alpha_t |u_c| u_c$ as an x-momentum source term, and the given surface-layer 'wall function.'

ACKNOWLEDGEMENTS

The authors gratefully acknowledge the Office of Naval Research for its financial support of this research (Award No. N00014-17-1-2102), and the reviewers for their helpful comments.

References

B. Aupoix. A general strategy to extend turbulence models to rough surfaces: Application to smith's $k-l$ model. *J. Fluids Eng.*, 129:1245–1254, 2007.

G. J. Brereton, M. Aghaei Jouybari, and J. Yuan. Towards modeling of turbulent flow over surfaces of arbitrary roughness. *Phys. Fluids*, 33:065121–1—13, 2021.

D. Chung, L. Chan, M. MacDonald, N. Hutchins, and A. Ooi. A fast direct numerical simulation method for characterising hydraulic roughness. *J. Fluid Mech.*, 2015.

C. F. Colebrook. Turbulent flow in pipes with particular reference to the transition region between smooth- and rough-pipe laws. *J. Inst. Civ. Eng.*, 11:133–156, 1939.

P. A. Durbin and B. A. Pettersson Reif. *Statistical theory and modeling for turbulent flows*. Wiley, 2001.

J. Jimenez and P. Moin. The minimal flow unit in near-wall turbulence. *J. Fluid Mech.*, 225:213–240, 1991.

T. Knopp, B. Eisfeld, and J. B. Calvo. A new extension for $k-\omega$ turbulence models to account for wall roughness. *Int. J. Heat Fluid Flow*, 30:54–65, 2009.

M. MacDonald, D. Chung, N. Hutchins, L. Chan, A. Ooi, and R. García-Mayoral. The minimal-span channel for rough-wall turbulent flows. *J. Fluid Mech.*, 816:5–42, 2017.

C. Meneveau. A note on fitting a generalised moody diagram for wall modelled large-eddy simulations. *J. Turbul.*, 21:650–673, 2020.

J. Nikuradse. Laws of flow in rough pipes. *NACA Technical Memorandum 1292*, 1933.

M. R. Raupach and R. H. Shaw. Averaging procedures for flow within vegetation canopies. *Bound.-Lay. Meteorol.*, 22:79–90, 1982.

N. Saito, D. I. Pullin, and M. Inoue. Large eddy simulation of smooth-wall, transitional and fully rough-wall channel flow. *Phys. Fluids*, 24:075103, 2012.

R. P. Taylor, H. W. Coleman, and B. K. Hodge. Prediction of turbulent rough-wall skin friction using a discrete element approach. *J. Fluids Eng.*, 107: 251–257, 1985.

J. Varghese and P. A. Durbin. Representing surface roughness in eddy resolving simulation. *J. Fluid Mech.*, 897:A10–1–23, 2020.

D. C. Wilcox. Turbulence modeling for CFD. DCW Industries Inc., La Canada, CA, 1993.

J. Yuan and U. Piomelli. Roughness effects on the Reynolds stress budgets in near-wall turbulence. *J. Fluid Mech.*, 760:R1, 2014.